

RESEARCH

Open Access



Deletion of exons 45 to 55 in the *DMD* gene: from the therapeutic perspective to the in vitro model

Javier Poyatos-García^{1,2,3*}, Patricia Soblechero-Martín⁴, Alessandro Liquori^{5,6}, Andrea López-Martínez⁴, Pilar Maestre¹, Elisa González-Romero⁵, Rafael P. Vázquez-Manrique^{7,8,9}, Nuria Muelas^{1,10,11}, Gema García-García^{7,8,9}, Jessica Ohana¹², Virginia Arechavala-Gomez^{4,13†} and Juan J. Vilchez^{1,3,10,11*†}

Abstract

Background Gene editing therapies in development for correcting out-of-frame *DMD* mutations in Duchenne muscular dystrophy aim to replicate benign spontaneous deletions. Deletion of 45–55 *DMD* exons (del45–55) was described in asymptomatic subjects, but recently serious skeletal and cardiac complications have been reported. Uncovering why a single mutation like del45–55 is able to induce diverse phenotypes and grades of severity may impact the strategies of emerging therapies. Cellular models are essential for this purpose, but their availability is compromised by scarce muscle biopsies.

Methods We introduced, as a proof-of-concept, using CRISPR-Cas9 edition, a del45–55 mimicking the intronic breakpoints harboured by a subset of patients of this form of dystrophinopathy (designing specific gRNAs), into a Duchenne patient's cell line. The edited cell line was characterized evaluating the dystrophin expression and the myogenic status.

Results Dystrophin expression was restored, and the myogenic defects were ameliorated in the edited myoblasts harbouring a specific del45–55. Besides confirming the potential of CRISPR-Cas9 to create tailored mutations (despite the low cleavage efficiency of our gRNAs) as a useful approach to generate in vitro models, we also generated an immortalized myoblast line derived from a patient with a specific del45–55.

Conclusions Overall, we provide helpful resources to deepen into unknown factors responsible for *DMD*-pathophysiology.

Keywords Duchenne muscular dystrophy, Becker muscular dystrophy, CRISPR-Cas9, Gene therapy, Cell model, Dystrophin

[†]Virginia Arechavala-Gomez and Juan J. Vilchez are senior authors.

*Correspondence:

Javier Poyatos-García

javier.poyatos@uv.es

Juan J. Vilchez

juan.vilchez@uv.es

Full list of author information is available at the end of the article



© The Author(s) 2024. **Open Access** This article is licensed under a Creative Commons Attribution-NonCommercial-NoDerivatives 4.0 International License, which permits any non-commercial use, sharing, distribution and reproduction in any medium or format, as long as you give appropriate credit to the original author(s) and the source, provide a link to the Creative Commons licence, and indicate if you modified the licensed material. You do not have permission under this licence to share adapted material derived from this article or parts of it. The images or other third party material in this article are included in the article's Creative Commons licence, unless indicated otherwise in a credit line to the material. If material is not included in the article's Creative Commons licence and your intended use is not permitted by statutory regulation or exceeds the permitted use, you will need to obtain permission directly from the copyright holder. To view a copy of this licence, visit <http://creativecommons.org/licenses/by-nc-nd/4.0/>.

Background

Dystrophinopathies encompass a series of muscular disorders caused by mutations in the *DMD* gene leading to structural or functional alterations in the protein dystrophin. Dystrophin is a member of the dystrophin-glycoprotein complex located in the sarcolemma, which connects the actin cytoskeleton to the extracellular matrix, conferring structural stability to the muscle fibres during contraction and playing an important role in cellular signalling [1, 2]. The diverse phenotypic manifestations of these disorders underscore the involvement of disparate pathomechanisms, the comprehension of which is vital for the development of targeted medical management and treatment strategies for this category of degenerative diseases.

The most severe and prevalent phenotype consists in Duchenne muscular dystrophy (DMD), affecting 1 out of 3500–5000 newborn males [3–5], and is mainly caused by frame-disrupting *DMD* mutations. It is characterized by progressive skeletal muscle degeneration from early childhood, resulting in the loss of ambulation by the age of 13 and early death in the thirties due to respiratory and cardiac complications. Conversely, mutations that maintain the *DMD* open reading frame (ORF) permit the production of partially functional dystrophins, typically resulting in Becker muscular dystrophy (BMD). BMD is characterised by the ability to walk beyond the age of 16 years and a broader spectrum of age of onset and severity of muscle weakness [5] and with an incidence of 1 in 18,500 live male births [6]. Other phenotypes associated with *DMD* mutations include isolated hyperCKemia [7], the presence of pseudo-metabolic manifestations such as exercise-induced myalgia and rhabdomyolysis [8], isolated cardiomyopathy [9], and cognitive and neurodevelopmental abnormalities that are typically associated to the aforementioned phenotypes [10]. In addition to the impact of each mutation on ORF, the clinical severity is also contingent upon the alteration of the conformational structure of the resulting dystrophin, which can impede its proper assembly and interaction with other proteins [11]; and the influence of *trans* gene modifying factors [12].

Currently, there is no effective cure for DMD but several potential therapies addressing both the primary defect (lack of dystrophin) and secondary pathology (as consequence of its deficiency) are in advance stages of clinical testing [13, 14]. Among them, exon skipping and microdystrophin gene transfer are promising therapeutic approaches based on the restoration or replacement of the dystrophin functionality. Exon skipping can be achieved by restoring the reading frame using splice-switching antisense oligonucleotides (AONs) acting on pre-mRNA to promote the skipping of the targeted exon [15], or by gene editing technologies acting on the DNA

producing a permanent excision of the exon (s) of interest [16–19]. To date, four AONs have already received FDA (United States Food and Drug Administration) approval: eteplirsen, golodirsen, vitolarsen and casimersen (skipping exons 51, 53 and 45 respectively) [14]. Conversely, genomic technologies to assemble crucial functional protein domains into constructs suitable for delivery by viral vectors are employed in microdystrophin gene transfer therapy [20]. A major milestone for this strategy is the recent FDA approval of Elevidys, the first gene therapy for DMD [14]. Despite these promising clinical and preclinical results, it remains essential to overcome significant hurdles such as specificity, efficiency, immunogenicity, and delivery issues to transform these approaches into viable therapeutic options [13, 14, 21]. In this regard, the analysis of BMD patients or other benign dystrophinopathy phenotypes with in-frame deletions that mimic those achieved by exon skipping is essential to predict the therapeutic potential of these approaches [22, 23].

Among the various mutations observed along the *DMD* gene, the deletion of exons 45–55 (del45–55) has been proposed as a promising therapeutic model with the potential to correct up to 47% of the total *DMD*-causing mutations [24–26]. This in-frame deletion in the central dystrophin rod domain, formerly reported as benign, has also been demonstrated to be a causative factor in significant functional impairment, severe cardiac complications, cognitive alterations, and potential shortening of life expectancy [27]. Nevertheless, despite an exhaustive search for potential *DMD cis* alterations (including intronic breakpoint positions disrupting regulatory sequences located in introns 44 and 55) and the effects of *trans* modifying factors, the underlying pathomechanisms remain elusive [27]. Therefore, although functional dystrophin has been successfully restored in cellular and animal *DMD* models through the skipping of exons 45–55, using both cocktails of AONs [28–31] and CRISPR-Cas9 gene editing [32–34], further investigation of this deletion is necessary to establish this model as an effective therapeutic alternative.

In this context, cellular models are of paramount importance, not only for the investigation of unidentified molecular mechanisms that contribute to the physiopathology, but also for the development of new therapeutic strategies in preclinical stages. The most reliable cellular models are primary human myoblasts isolated from patient muscle biopsies, as they present the natural genomic background of the disease. However, they have limited proliferative capacity, which is associated with cellular senescence. To address these challenges, the immortalisation of myogenic human cell lines has emerged as a crucial tool in the investigation of neuromuscular disorders. These immortalised cell lines exhibit enhanced proliferative capacity while retaining the

differentiation potential and myogenic expression pattern observed in primary cells [35, 36]. Nevertheless, in many hereditary neuromuscular disorders, muscle biopsies are not performed for diagnostic purposes due to the advance of next-generation sequencing (NGS) methods and the consequent limitation of available cell lines, particularly those of a specific mutation. To address this issue, the CRISPR-Cas9 system has emerged as a valuable approach for creating custom cell disease cell lines and expanding the models available for the research of human neuromuscular diseases [37].

In this study, we evaluated, as a proof of concept, the replication of the intronic breakpoint positions of a subgroup of del45–55 patients previously analysed [27], using the CRISPR-Cas9 gene editing tool, as an attractive approach to restore the *DMD* reading frame of a DMD cell line. This strategy may also prove useful in generating cell models with specific deletions, which could facilitate further investigation into novel disease pathomechanisms. Furthermore, an immortalised cell line derived from an asymptomatic patient harbouring the specific del45–55 was characterised.

Methods

Cell cultures and myoblasts immortalization

HEK293 cells were maintained with Dulbecco's modified Eagle Medium high glucose (DMEM), supplemented with 10% Foetal Bovine Serum and 1% of penicillin-streptomycin (Thermo Fisher, Waltham MA, USA).

A myoblast immortalised DMD cell line with a deletion of exon 52 (DMD Δ 52) (ID: DMD638a) was provided by the Institute of Myology (Paris, France) and was the subject of the CRISPR/Cas9 gene edition. Additionally, immortalised human myoblasts derived from three healthy male donors' biopsies (ID: AB1079 (C1), AB1190 (C2) and AB678 (C3) of 38, 16 and 53 years old respectively) were also provided by the Institute of Myology.

To create an immortalised culture (named Im Δ 45–55-D1), a biopsy of *tibialis anterior* from a 32-year-old male donor harbouring a del45–55 with specific intronic breakpoints (del45–55-D1), was obtained in La Fe University Hospital (Valencia, Spain) after informed consent (research ethics committee authorization 2018/0200). Primary human skeletal myoblasts were purified as previously described [38] and immortalized in collaboration with the Institute of Myology (Paris, France) to increase its proliferative capacity as follows: primary myoblasts were transduced with both hTERT and Cdk4 lentiviral vectors with a ratio of the number of transducing lentiviral particles to the number of cells (MOI) of 5 in the presence of 4 μ g/ml of polybrene (Sigma-Aldrich, Sant Luis, MO, USA). Transduced cell cultures were selected with puromycin (0.2 μ g/ml, Life Technologies, Carlsbad, CA, USA) for four days and neomycin (0.3 mg/ml, Life

Technologies, Carlsbad, CA, USA) for ten days. Cells were seeded at clonal density and selected clones were isolated from each population using glass cylinders [36].

Human myoblasts were cultured with Skeletal Muscle Cell Growth Medium (SMC) (PELOBiotech, Planegg, Germany). Differentiation medium (DM), when needed, was prepared with DMEM, supplemented with 2% of Horse Serum and 1% of penicillin-streptomycin (Thermo Fisher, Waltham MA, USA).

Cell proliferation assay

A total of 5000 primary and immortalized myoblasts (derived from the patient 45–55) per well were seeded in 96-well plates and were incubated at 37° C in a humidified chamber with 5% CO₂ for 24, 48, 72, and 96 h in SMC medium. Cell proliferation was measured using the CellTiter 96 aqueous non-radioactive cell proliferation assay (MTS) (Promega, Madison, WI, USA) as previously described [39].

CRISPR-Cas9 design and gRNA selection

Two gRNAs were designed to target the vicinity of each breakpoint in intron 44 and 55 of the del45–55-D1 (ChrX:32056814 and ChrX:31599476 respectively, according to the human genome reference GRCh37/Hg19), using the Zhang lab designing tool (crispr.mit.edu). The genomic location and the sequence of the four gRNAs can be found in Table S1.

Each gRNA was cloned into a plasmid containing spCas9 and EGFP sequences (PX458; Addgene 48138) [40]. To assess the cleavage efficiency of the sgRNAs, 1.5ug of each plasmid was transfected independently into HEK293 cells using Lipofectamine 3000 (Invitrogen, Carlsbad, CA, USA). Forty-eight hours after transfection, the genomic DNA was extracted (QIAamp® DNA Mini Kit, Qiagen) amplified using primers hybridising in the proximity of the cleavage site (Table S1), and the PCR products were purified. The T7E1 assay was then performed and indel frequencies were calculated as previously reported [41].

The two selected gRNAs (gRNAs_{44.1} and 55.2), targeting intron 44 and 55 breakpoints) were co-transfected into HEK293 cells (1.5ug of each plasmid) to evaluate the production of the *DMD* del45–55-D1. Forty-eight hours after co-transfection, cells' DNA was extracted and amplified by PCR (using Δ 45–55-D1 screening primers) and subsequently sequenced using Sanger sequencing (Table S1).

Generation of edited clones with the del45–55-D1 (Edited Δ 45–55)

The immortalised DMD Δ 52 myoblasts were co-transfected with 1.5ug of each plasmid containing the selected sgRNAs using Viafect™ (Promega, Madison, WI, USA)

transfection reagent (1:5 ratio). Forty-eight hours after transfection, fluorescence activated cell sorter (FACS) was applied to seed individually the GFP positive cells into 96 well plates and amplified to form homogeneous clonal cell cultures as previously described [37]. The DNA was extracted from the successfully grown clones, analysed by PCR and resolved on a 1% agarose gel to detect those harbouring the del45–55-D1 (Table S1). One edited clone, named “Edited Δ 45–55” was expanded for further for characterisation analysis. These experiments were carried out at Biobizkaia HRI, Barakaldo, Spain (NAT-RD group).

On-target and off-target analysis

In order to identify any potential off-targets that might be produced by the gRNAs_44.1 and 55.2 (containing up to three mismatches), Cas-OFFinder tool was employed [42].

Amplicon high-throughput sequence analysis was conducted to evaluate the on-target efficiencies and the potential off-target events. The off-target analysis was conducted using DNA from DMD immortalised myoblasts that had been co-transfected with both sgRNAs. For the on-target analysis DNA from DMD myoblasts transfected with the sgRNA of interest (either 44.1 or 55.2) was used in each case. DNA from DMD untransfected myoblasts was used as control for each target locus. A two-step PCR strategy was employed to generate the library. For the first PCR (PCR1), primers for each locus contained an adapter sequence. PCR products were purified using AMPure Beads (BD Bioscience, Franklin Lakes, NJ, USA). For the second (PCR2), PCR products were re-amplified with primers containing the adapter sequence overlapping the first primers, and with an index sequence in the reverse primer. Final PCR products were purified with AMPure Beads. The library was prepared with the PCR products pooled in equimolar amounts following the manufacturer’s protocol, and loaded in a Micro MiSeq Reagent Kit v2 (500-cycles) (Illumina, San Diego, CA, USA) on a MiSeq platform (Illumina). The fastq.gz files were analysed using the CRISPResso2 software to evaluate the edition efficiency and potential off-target effects, using default parameters. The primers used for the PCR1 and PCR2 are listed in Table S2.

Additionally, we analysed the potential off-targets of the selected clone used for the functional characterisation by Sanger sequencing (using PCR1 primers without the adapter sequence, Table S2).

RNA analysis

RNA was extracted from differentiated cell cultures (at day 0, 2, 5 and 7 of differentiation) after being pelleted (RNeasy mini kit, Qiagen, Hilden, Germany). Reverse transcription was performed using 1 μ g of total RNA and

with SuperScript IV Reverse Transcriptase (Invitrogen, Waltham, MA, USA) and nested PCR of cDNA samples was carried out using specific primer pairs (hybridising in DMD exons 41 and 60 (RT-PCR1) and in exons 43 and 59 (RT-PCR2); Table S1) as previously described [27]. The PCR products were analysed on 1% agarose gels, DNA was purified (Gel Extraction Kit; Omega Bio-Tek, Norcross, GA, USA) and validated via Sanger sequencing.

Duplex droplet digital PCR (ddPCR) was performed with 2 μ l of cDNA using the QX200 Droplet Digital PCR system (Bio-Rad Laboratories, Hercules, CA, USA), as previously described [27] for the detection of: dystrophin (probe ID: dHsaCPE5049433, HEX labelled, Bio-Rad), Pax7 (probe ID: Hs.PT.58.19502533, FAM labelled, IDT); Myf5 (probe ID: Hs.PT.58.20820798, FAM labelled, IDT); MyoD (probe ID: Hs.PT.58.39155876, FAM labelled, IDT) and Myh3 (probe ID: Hs.PT.58.45297783, HEX labelled). TBP (probe ID: Hs.PT.58v.39858774, HEX labelled, IDT) and HPRT1 (probe ID: Hs.PT.58v.45621572, FAM labelled, IDT) were used for expression normalisation.

Cell cultures immunofluorescence

For all immunodetections, 2.5×10^4 myoblasts /well were seeded in 24-well plates and, after 0, 2, 5 and 7 days differentiating into myotubes, cells were fixed in 4% paraformaldehyde. The cell cultures were permeabilised with PBS-T (0.1% X-TritonX-100 in PBS 1X) and blocked for 1 h at room temperature (RT) in PBS-T, 1% BSA, 1% normal goat serum (blocking buffer) before incubation with primary antibodies, diluted in blocking buffer, overnight at 4 °C. For dystrophin immunostaining, a mixture of three mouse monoclonal antibodies at 1:50 dilution was used: NCL-Dys1 (Novocastra Laboratories, Newcastle Upon Tyne, UK), Mandys1 and Mandys106 (The Wolfson Centre for Inherited Neuromuscular Disease). For myosin heavy chain detection (MyHC), a mouse monoclonal anti-MyHC antibody was used (MF20, 1:50, DSHB, University of Iowa, IA, USA) and for desmin detection, a rabbit polyclonal anti-desmin antibody (1:200, Abcam, Cambridge, UK) was utilised. Following a PBS-T wash, cells were incubated with the appropriate secondary antibody: goat anti-Mouse IgG (H+L) Alexa Fluor Plus 488 and goat anti-rabbit IgG (H+L) Alexa Fluor Plus 488 (1:200, Thermo Fisher). Subsequently, samples were mounted with VECTASHIELD® mounting medium containing DAPI (Vector Laboratories, London, UK) for the detection of the nuclei. Images were acquired in an LSM800 confocal microscope (Zeiss) at 100x magnification.

The fusion index was calculated as the percentage of nuclei within myotubes (>2 nuclei) out of the total number of nuclei in Desmin-positive cells (10 micrographs per condition), and the myotube diameter was calculated in parallel. The differentiation index was calculated as the

percentage of nuclei within MyHC-positive myotubes out of the total of nuclei (10 micrographs per condition) as we previously described [39].

Protein quantification

In-cell western assays (myoblots) were performed as previously described [43, 44]. Briefly, the cultures were seeded in 96-well plates and differentiated for 7 days. Plates then were fixed with ice-cold methanol, permeabilised with PBS-T, blocked (Intercept (PBS) blocking buffer, LI-COR® Biosciences, Lincoln, NE, USA) and incubated with primary antibodies overnight at 4°C. For dystrophin detection, the mixture of the three primary antibodies described above (NCL-Dys1, ManDys1 and ManDys106, 1:100 each) was used. On the subsequent day, the plates were incubated with the secondary antibody. The secondary antibody, IRDye 800CW goat anti-mouse 1:500, was prepared together with CellTag 700 Stain (LI-COR® Biosciences) at 1:1000 dilution and incubated for 1 h at RT and protected from light. After incubation, plates were analysed using the Odyssey® M Imager (LI-COR® Biosciences).

Western blot quantification was performed on cultures seeded in P6 plates (2.5×10^5 cells/well) and differentiated for seven days. The cell pellets were then collected and solubilized in lysis buffer [45]. Protein concentration was determined using the BCA Protein Assay (Thermo Fisher, Waltham MA, USA). Samples were loaded onto a NuPAGE® Novex® 3–8% Tris-Acetate (Thermo Fisher, Waltham MA, USA) and run at 100 V during 5 h. Protein wet transference onto 0.45 µm nitrocellulose membrane was carried out at 20 V for 18 h at 4 °C. Then, membranes were blocked in 5% non-fat dry milk diluted in TBST (0.1% Tween20) for 1.5 h at RT and incubated overnight at 4°C with primary antibodies: anti-dystrophin antibody (NCL-Dys1, 1:40, Novocastra Laboratories) and anti-alpha actinin antibody (A7732, 1:3000, Sigma-Aldrich). The membranes were incubated with the secondary antibody sheep anti-mouse IgG (H+L) (ab6808, 1:2000, Abcam) for 1 h in dark. Membranes were revealed using SuperSignal™ West Pico PLUS (Thermo Fisher, Waltham MA, USA) using an Amersham Imager 600 (GE Healthcare, Chicago, IL) imaging system. Bands' intensities were quantified with the ImageJ software (NIH, Bethesda, MD, USA). The dystrophin signal was normalised to the alpha-actinin signal.

Statistical analysis

Mann–Whitney U, Kruskal–Wallis and linear regression tests were used to determine the statistical significance of the obtained data. Statistical analysis was performed using GraphPad Prism 6 software.

Results

Generation of del45–55-D1 immortalized cell model (ImΔ45–55-D1)

The manipulation of primary human myoblasts is a challenging process due to their low proliferative potential. Therefore, we elected to immortalise the primary cells from a 32-year-old male carrier with a del45–55 with specific intronic breakpoints. The patient was classified as asymptomatic despite presenting with elevated serum creatine kinase levels (2400 UI/L), as no signs of functional impairment were observed. This particular deletion of DMD exons 45 to 55 has been designated “del45–55-D1,” in accordance with the findings previously reported by our research group [27]. The culture derived from it has been designated “ImΔ45–55-D1”. Following immortalisation, the proliferation potential of the primary and immortalised cell lines was analysed at 24, 48, 72 and 96 h. This confirmed that the immortalised line exhibited significantly greater proliferation than the primary one (Fig. S1).

Generation of edited myoblasts clones mimicking the specific del45–55-D1 (EditedΔ45–55)

We employed the CRISPR-Cas9 gene editing method to restore dystrophin expression in an immortalised DMD cell line with a deletion of exon 52 (DMDΔ52) by replicating del45–55-D1. To demonstrate the efficacy of this approach for generating cell models, we compared the generated cell culture, designated “EditedΔ45–55,” with the immortalized myoblasts carrying the same mutation (ImΔ45–55-D1). In order to achieve this objective, two CRISPR gRNAs targeting each intronic breakpoint were designed and cloned into plasmid vectors expressing the Cas9 nuclease and GFP (Table S1). The four plasmids containing each gRNA were transfected individually into HEK293 cells, and their cleavage efficiencies were evaluated using the T7E1 assay. Based on the estimated indel frequencies (Fig. S2), we selected the sequences gRNA_44.1 and gRNA_55.2 (targeting intron 44 and 55 breakpoints, respectively) for the generation of the edited clones. The two plasmids were co-transfected into HEK293 cells, thereby confirming the production of the del45–55-D1. The location of the deletion across introns 44 and 55, along with the sequences and design of the gRNAs, are illustrated in Fig. 1A and B.

Subsequently, the plasmids containing the selected gRNAs were co-transfected into the target immortalised human DMDΔ52 myoblasts. Two days following transfection, cells exhibiting GFP expression, indicative of vector incorporation, were sorted by FACS and seeded individually into 96-well plates. This process was undertaken to facilitate the generation of homogeneous clonal cell cultures. The clones were expanded and screened by PCR and Sanger sequencing, with approximately one

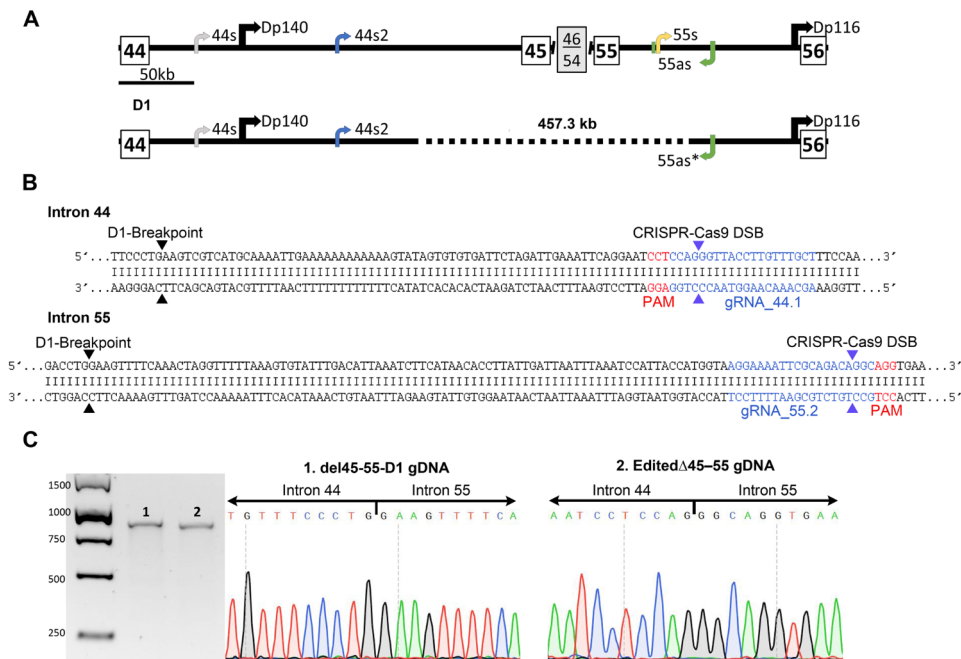


Fig. 1 CRISPR-Cas9 design based on the location of the del45–55-D1 breakpoint. **(A)** the upper part of the image depicts the genomic architecture along introns 44 and 55 illustrating the relative position of the promoter of the Dp140 and Dp116 dystrophin isoforms, as well as the location of the lncRNA 44s, 44s2, 55s and 55as. The figure below depicts the specific breakpoints in introns 44 and 55 of the D1 deletion group (del45–55-D1), illustrating their impact on the aforementioned elements (dotted lines indicate the deleted region). **(B)** the genomic sequences of introns 44 and 55 are illustrated, with the location of the patient breakpoints indicated by black arrowheads. The gRNAs targeting each intron are represented by blue letters, and their PAM (protospacer adjacent motif) sequences are indicated in red. Purple arrowheads indicate the location of the expected Cas9 DSB (double-strand break). **(C)** genomic sequences of the deletion junctions, confirmed by Sanger sequencing of (1) the patient harbouring this specific deletion and (2) the Edited Δ 45–55 clone

in ten identified as containing the specific del45–55-D1 (Fig. 1C). One positive clone was selected for further characterisation.

Cleavage efficiency and off-target events analysis

Amplicon deep sequencing analysis was conducted to quantify the cleavage efficiencies (on-targets) of the selected gRNAs (gRNA_44.1 and gRNA_55.2) and to evaluate the occurrence of unspecific cleavage (off-targets events). The potential off-targets associated with each gRNA were identified using the Cas-OFFinder and Breaking-Cas predictors [42, 46] (Table 1).

Extracted DNA from transfected and untransfected cultures was used to generate the amplicon sequencing libraries. The fastq.gz files from the Miseq sequencer (Illumina) were analysed with the CRISPResso2 software [47] which employs a narrow window, restricted to the expected cleavage site, to quantify the DNA modifications (insertions, deletions and substitutions).

All amplicons (from both transfected and untransfected cells) exhibited high coverage (above 400,000 properly aligned reads) with the exception of the gRNA_44.2 off-target 3 amplicon, which did not meet the software coverage requirements for its analysis. It is possible that this discrepancy may have arisen due to an error in the determination of the concentration of this particular amplicon,

which may have subsequently affected the composition of the final pool. Table S3 illustrates the number of reads classified according to each DNA modification for each analysed amplicon. Regarding the on-target, we observed a 5.50% and a 9.99% of modified reads associated with the gRNA_44.1 and 55.2, respectively. In both cases, the majority of modifications corresponded to indels, which are characteristic of the NHEJ repair pathway (Fig. 2).

Furthermore, the seven potential off-targets were analysed in the Edited Δ 45–55 clone used for functional characterisation assays through PCR followed by Sanger sequencing. No off-target effect was identified at any locus analysed (Fig. S4).

Dystrophin expression is recovered in the Edited Δ 45–55 clone

The objective of this study was to ascertain whether the generation of the specific del45–55-D1 could serve to restore the *DMD* reading frame of a DMD Δ 52 cell line, thereby enabling dystrophin production. Furthermore, we propose a valuable approach to compare the edited cell line to the immortalised myoblasts from the patient harbouring this specific deletion (Im Δ 45–55-D1). Additionally, the original immortalised cell lines, DMD Δ 52 and control (C1), were introduced for use in these experiments.

Table 1 Sequence and genomic location of the on-target and potential off-targets regions

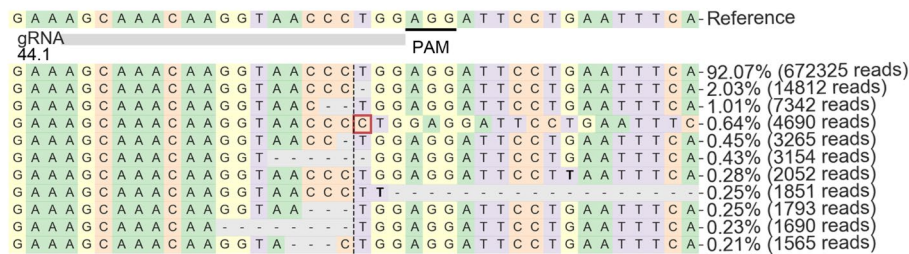
Name	Location ^a	Gene ^b	Sequence (5'-3') ^c
gRNA_44.1 On	ChrX: 32,038,608–32,038,631 (+)	<i>DMD</i> (ENSG00000198947)	AGCAAACAAGGTAACCTGG AGG
gRNA_44.1 Off1	Chr2:105083351–105,083,374 (-)	<i>MRPS9</i> (ENSG00000135972)	AGgAAAggAGGTAACCTGG TGG
gRNA_44.1 Off2	Chr2: 14,281,851–14,281,874 (+)	<i>LINC00276</i> (ENSG00000230448)	AtCcAAACAgaTAACCTGG GGG
gRNA_44.1 Off3	Chr9: 21,835,997–21,836,020 (-)	<i>MTAP</i> (ENSG00000099810)	AGCAAAGAgGGTAgCCCTGG GGG
gRNA_55.2 On	ChrX: 31,581,248–31,581,271 (-)	<i>DMD</i> (ENSG00000198947)	AGGAAAATTCGACAGCAGGC AGG
gRNA_55.2 Off1	Chr5: 157,057,959–157,057,982 (+)	<i>HAVCR1</i> (ENSG00000113249)	AGGAAAATgaGCAGACAGGCT TGG
gRNA_55.2 Off2	Chr11: 94,916,762–94,916,785 (+)	<i>lncRNA</i> (ENSG00000256469)	AGGAAAATTaCAGACAGGa TGG
gRNA_55.2 Off3	Chr6: 111,393,626–111,393,649 (-)	<i>REV3L</i> (ENSG00000009413)	AGGAAGATaCGaAGACAGGCT TGG
gRNA_55.2 Off4	Chr2: 238,379,513–238,379,536 (-)	<i>TRAF3IP1</i> (ENSG00000204104)	AGGAAAATTCaCaTACAGGa TGG

(a) Genomic location based on reference human genome GRCh38/hg38

(b) Gene name and Ensembl accession code

(c) Nucleotides in minor letters indicate its discrepancy with the original gRNA sequence (mismatches). The PAM sequence (protoespacer adjacent motif) is indicated in bold

A



B

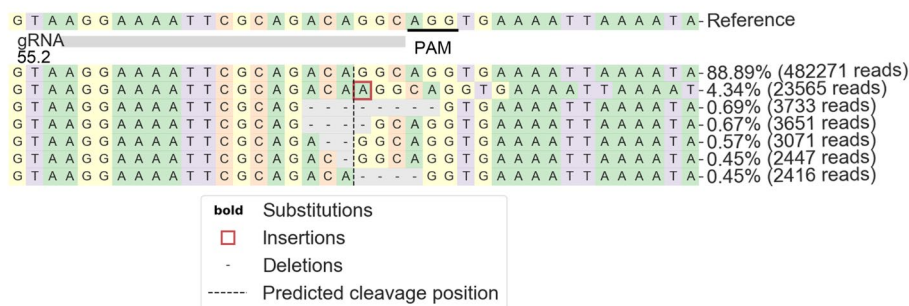


Fig. 2 Summary of the principal allele frequencies generated after the gRNAs cleavages. Representation of the NGS reads frequencies derived from the transfection of gRNA44.1 (A) and gRNA55.2 (B). The reference sequence is indicated along with the principal modifications, where percentage is indicated. The image has been adapted from the results obtained with the CRISPResso2 program. The figure legend explains the produced changes and the expected Cas9 cleavage site. Conversely, the CRISPResso2 Compare software was employed to examine off-target events. This software analyses the outcomes of the transfected and untransfected samples in relation to the reference sequence for each amplicon (Fig. S3). No indel event was identified in any of the transfected samples in the vicinity of the anticipated cleavage site. Nevertheless, we did discern the existence of substitutions, which, in select instances (gRNA_44.1 off-target 1 and gRNA_55.2 off-target 4), exhibited a heightened prevalence in the untransfected sample. The presence of substitutions was observed in the transfected sample of gRNA_44.1 off-target 2, although they were distant from the expected cleavage site (Fig. S3)

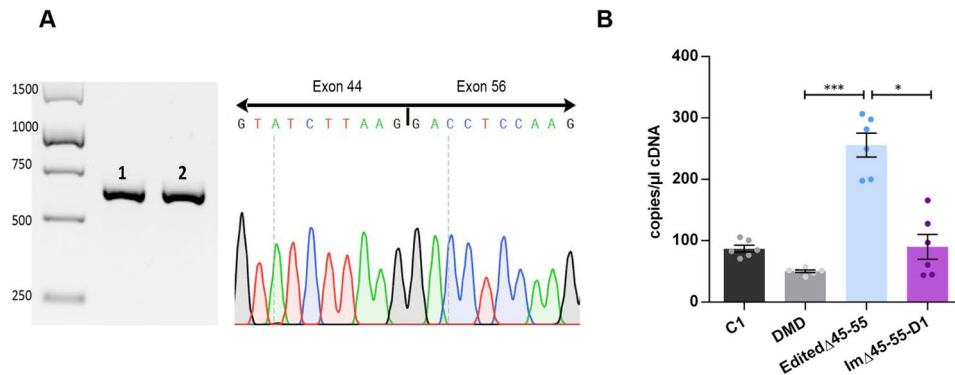


Fig. 3 Dystrophin cDNA expression analysis of the edited clone. **(A)** Confirmation of the del45–55-D1 of the differentiated myotubes cDNA from (1) the Im Δ 45–55-D1 and (2) from the Edited Δ 45–55 clone. In both samples the exon 56 sequence is juxtaposed to the exon 44 one. **(B)** Dystrophin expression quantification through ddPCR of the differentiated myotubes cDNA from Control (C1), unedited DMD, the Edited Δ 45–55 and the Im Δ 45–55-D1 cell lines ($n=8$ replicates). The bar graphs represent mean \pm SEM. * $p < 0.05$, *** $p < 0.001$, according to Kruskal-Wallis test

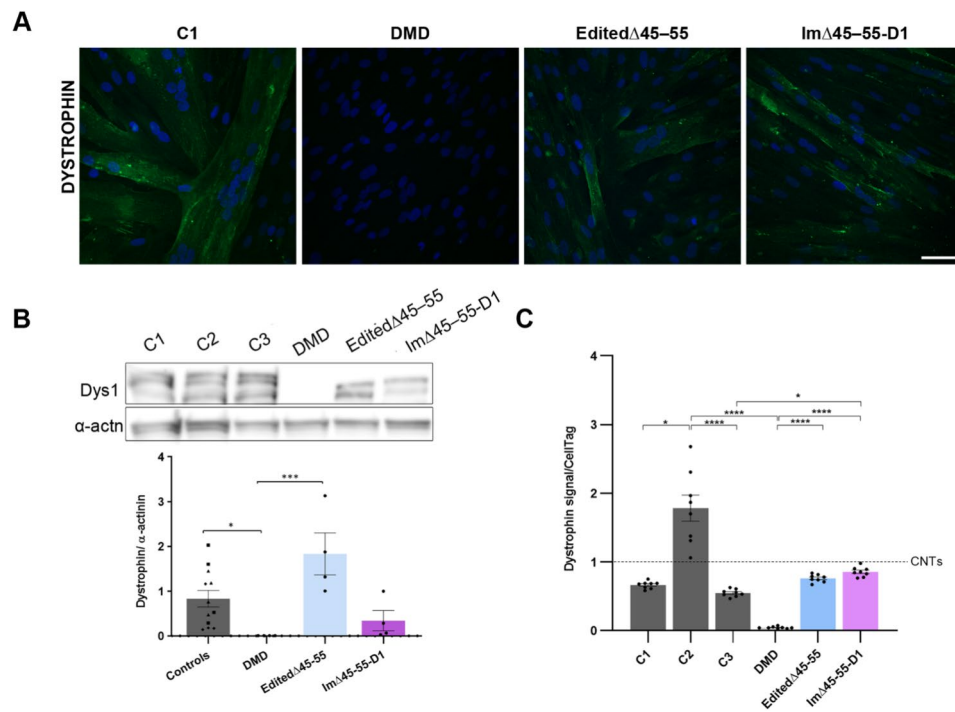


Fig. 4 Dystrophin evaluation of the edited clone myotubes. **(A)** Representative confocal images of dystrophin immunofluorescence (green) in differentiated myotubes from: Control (C2), DMD, Edited Δ 45–55 and Im Δ 45–55-D1. Nuclei were stained with DAPI (blue) (scale bar = 50 μ m). **(B)** Quantification and representative blots of dystrophin in protein extracts from 3 healthy controls (C1=▲, C2=■, C3=◆); DMD, the Edited Δ 45–55 and Im Δ 45–55-D1 myotubes. Dystrophin levels (Dys1) were normalized to α -actinin signal (α -actn) ($n=4$ technical replicates). **(C)** In-cell western quantification of dystrophin expression of three healthy controls (C1, C2, and C3), DMD, the Edited Δ 45–55 and Im Δ 45–55-D1. Dystrophin signal is normalised to cell number signal (Cell Tag) and set to 1 (mean of the three controls) ($n=6$ wells). * $p < 0.05$, *** $p < 0.001$, **** $p < 0.0001$ according to Mann-Whitney U **(B)** and Kruskal-Wallis **(C)** and error bars represent the mean \pm SEM

Firstly, RT-PCR Sanger sequencing of Edited Δ 45–55 differentiated myotubes cDNA confirmed the in-frame deletion of 11 exons at RNA level (comparable to the template Im Δ 45–55-D1 sequence) (Fig. 3A). Furthermore, the quantification of dystrophin cDNA demonstrated that the Edited Δ 45–55 clone exhibited a restoration of dystrophin expression when compared to the DMD unedited line, with levels that were even higher

than those observed in the control and Im Δ 45–55-D1 lines (Fig. 3B).

Subsequently, we proceeded to the dystrophin characterisation at the protein level. The immunofluorescence of the Edited Δ 45–55 differentiated myotubes demonstrated the restoration of dystrophin expression, and its proper localization (Fig. 4A). Western blot analysis was employed to assess dystrophin quantification in the four

aforementioned cell lines, with two additional control samples (C2 and C3). The dystrophin recuperation in the edited myotubes was confirmed, showing a tendency to higher levels than the Im Δ 45–55-D1 and the 3 controls myotubes' (grouped) (Fig. 4B). Additionally, a precise and robust quantification of dystrophin was conducted using the in-cell western technique to reduce the observed variability with western blot. As illustrated in Fig. 4C, dystrophin expression in the Edited Δ 45–55 myotubes was restored, exhibiting now similar levels to those of the Im Δ 45–55-D1 myotubes. Furthermore, variable levels of dystrophin expression were noted among different healthy controls (Fig. 4C).

The introduction of the del45–55-D1 by CRISPR-Cas9 rescues the myoblasts differentiation defects of DMD cells

Myoblasts derived from DMD patients harbouring out-of-frame mutations preventing dystrophin production, demonstrate significant deficits in their capacity for differentiation [37]. In order to evaluate this process in the four cell lines, an analysis of the myoblasts' fusion capacity was conducted at differentiation times of 0, 2, 5 and 7 days. The fusion index and myotube diameter were determined in parallel at the aforementioned time points using desmin immunofluorescence, which allows for the identification of a muscle-specific type III intermediate filament. The results demonstrated that the fusion index of DMD myotubes was significantly reduced in comparison to that of the healthy control at all differentiation days. This parameter was restored in the Edited Δ 45–55 myotubes, which exhibited a comparable developmental trajectory to the Im Δ 45–55-D1 myotubes. Regarding the myotube diameter, we observed a delay in the increase in the Edited Δ 45–55 myotubes' which was boosted at d7 (Fig. 5A, B).

Furthermore, myosin heavy chain (MyHC) immunofluorescence was conducted as a late-differentiation marker [48] in the differentiated myotubes of the 4 cell lines at the 4 designated differentiation time points. The differentiation defects in the DMD myotubes were confirmed, with a notable absence of nuclei in MyHC+ cells at d2, reaching a maximum of 10% of the nuclei at d5. Conversely, the Edited Δ 45–55 line demonstrated an improvement in this parameter from d5, reaching 30% of the nuclei at d7, which was comparable to the patient-derived Im Δ 45–55-D1 myotubes (Fig. 5C, D).

To gain further insight into the differentiation process, a detailed evaluation of the expression of key myogenic factors was conducted across the entire differentiation time frame: Pax7, Myf5 (myogenic factor 5), MyoD (myoblast determination protein 1), as well as the late myogenic differentiation marker Myh3 (myosin heavy chain 3) across differentiation time [49].

The expression of Pax7, a specific marker of satellite cells was not detected in any cell line at any time. This finding aligns with prior observations that Pax7 may not be expressed in human immortalised myoblasts (data not shown) [50].

As expected, all cell lines exhibited elevated Myf5 levels at d0, consistent with its expression in proliferating myoblasts (Fig. 6A). Myf5 levels decreased drastically by d2, which coincided with the peak expression of MyoD. MyoD expression is critical for the initiation of myogenic differentiation and its levels decrease as the process progresses. It is noteworthy that MyoD levels at d5 in the DMD line were higher than in the other cell lines, which could indicate a defect in the final maturation of myotubes (Fig. 6B). Conversely, Myh3 levels increased during the differentiation process, with lower levels observed in the DMD line compared to the other cell lines, particularly at d5 when compared to the Edited Δ 45–55. By d7, Myh3 levels exhibit a slight decline in the DMD, Edited Δ 45–55, and Im Δ 45–55-D1 lines. However, in the latter two lines, levels remain higher (though not significantly) than in the DMD line (Fig. 6C).

Discussion

The large in-frame deletion encompassing *DMD* exons 45 to 55 has been postulated as a promising model for DMD therapy. This approach could be advantageous for a significant number of DMD patients with diverse mutations, potentially leading to either asymptomatic advancement or the emergence of benign phenotypes. Furthermore, the resulting dystrophin retains its filamentous structure and functionality despite the absence of spectrin repeats in the central rod domain [11]. However, this mutation is also associated with severe phenotypes, the aetiology of which remains largely unresolved. In this study, we sought to replicate a del45–55 with specific intronic breakpoints (del45–55-D1) as a proof of concept to recover dystrophin expression in a DMD Δ 52 immortalised myoblast using the CRISPR-Cas9 system. This specific mutation was present in a significant number of patients, due to two founder events, and was associated with a predominance of asymptomatic phenotypes [27]. Furthermore, this strategy enabled the generation of a custom cell model (Edited Δ 45–55), which was characterised and compared to the immortalised myoblasts from one of the asymptomatic patients sharing these specific breakpoints (Im Δ 45–55-D1).

The del45–55-D1 consists on a 457.3 kb deletion, which preserves the promoters of the Dp140 and Dp116 dystrophin isoforms. Deletions disrupting the *Dp140* regulatory sequences in intron 44 have been associated to the risk of cognitive impairment and brain structural and functional abnormalities [51, 52]. In addition, this deletion

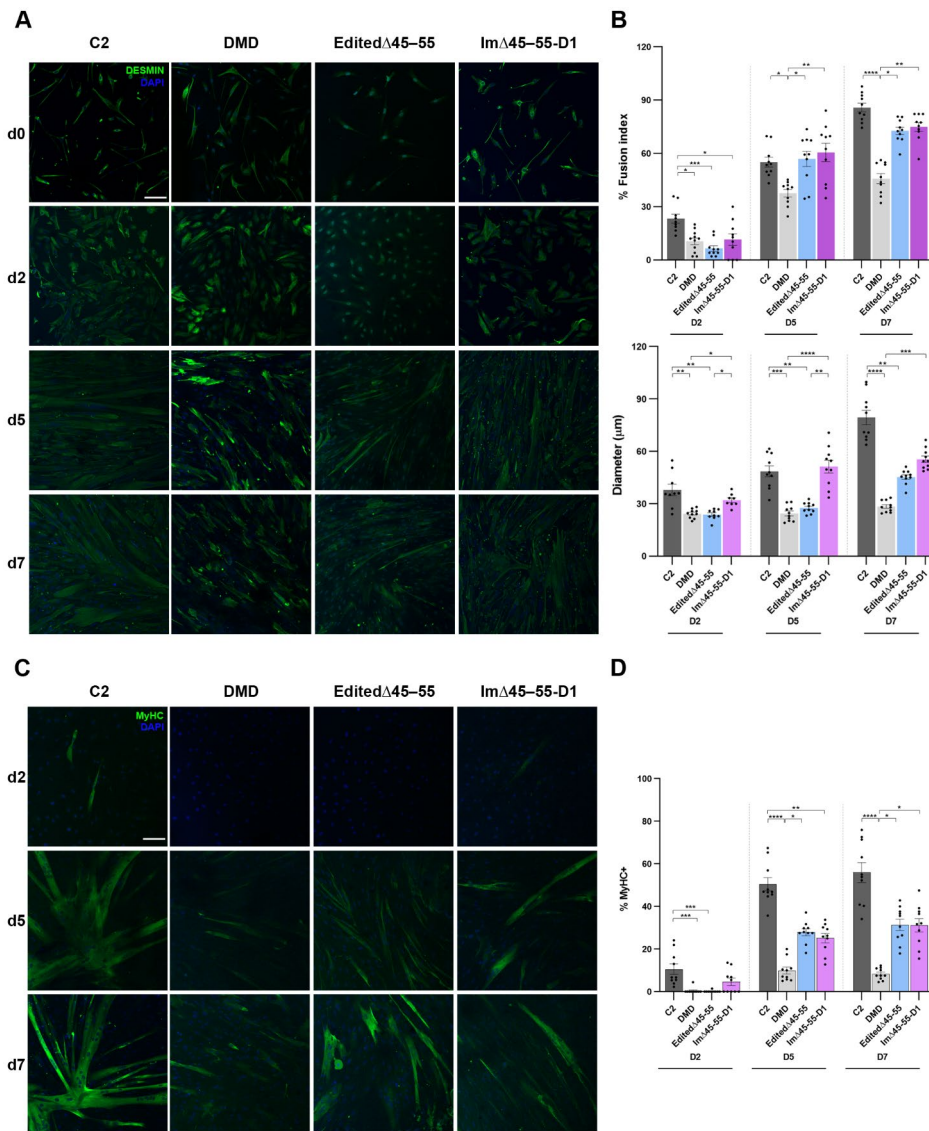


Fig. 5 Evaluation of the myogenic differentiation process after gene edition. Representative confocal images of Desmin **(A)** and MyHC **(C)** (myosin heavy chain) immunofluorescence (green) in control (C1), DMD, EditedΔ45–55 and ImΔ45–55-D1 at differentiation days 0, 2, 5 and 7 (d0, d2, d5, d7). D0 images of MyHC staining are not shown (negatively stained). Nuclei were stained with DAPI (blue) (scale bar = 50 μm). **(B)** Quantification of the myogenic fusion index and myotube diameter of the cell lines was calculated using the Desmin micrographs (10 images). **(D)** Quantification of the percentage of nuclei within MyHC + cells in each condition (10 images, 300–500 total nuclei). The bar graphs show the mean ± SEM; **p* < 0.05, ***p* < 0.01, ****p* < 0.001, *****p* < 0.0001, according to the Kruskal-Wallis test at each differentiation time point

conserved the expression of the lncRNAs, 44 and 44s2, reported as favourable by Gargaun and colleagues [53].

Although previous studies have also employed the CRISPR-Cas9 system to introduce the del45–55 [32, 33] they have inserted larger deletions (688 kb and 725 kb, respectively), being able to target a greater number of patients. However, these deletions are not based on natural models and may alter the regulatory elements located across introns 44 and 55, which could be relevant [54, 55].

Despite the successful reproduction of del45–55-D1 into a DMD cell line and the isolation of edited clonal

cell cultures, deep sequencing analysis revealed that the gRNA cleavage efficiencies were limited, as previously reported [37]. This poor on-target efficiencies may have been due to the difficulties encountered during transfection of the myoblasts [32, 56]. This is evidenced by the fact that less than 15% of the DMD myoblasts transfected with plasmids containing CRISPR-Cas9 elements and the GFP reporter expressed the reporter protein. Alternatively, other strategies, such as ribonucleoprotein (RNP) complexes, have demonstrated greater transfection and cleavage efficiencies, as well as reduced off-target effects, than plasmids (linked to the reduced time of active RNP

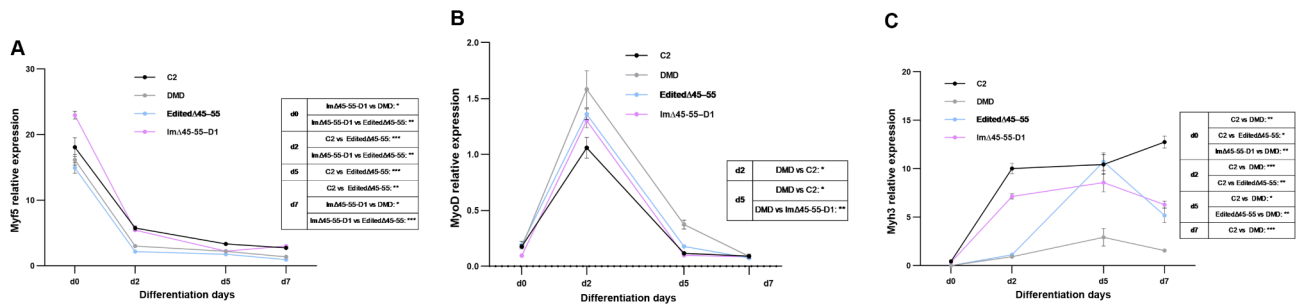


Fig. 6 Time course mRNA expression of myogenic markers during the differentiation process. The relative expression of Myf5 (A), MyoD (B) and Myh3 (C) was determined by ddPCR out at day d0, d2, d5 and d7 of differentiation in Control (C1), unedited DMD, the EditedΔ45–55 and the ImΔ45–55-D1 cell lines myotubes' cDNA ($n=6$ replicates). MyoD and Myf5 (FAM labelled) values were normalised to TBP (HEX labelled) while those for Myh3 (HEX labelled probe) to HPRT1 (FAM labelled). The error bars represent \pm SEM; * $p < 0.05$, ** $p < 0.01$, *** $p < 0.001$, **** $p < 0.0001$, according to the Kruskal-Wallis test at each differentiation time point

complexes compared to plasmids) [57, 58]. Indeed, our experience with RNPs in immortalised myoblast (at different loci) revealed cleavage efficiencies above 87% [39]. The efficient delivery of RNPs with non-viral vectors (such as nanoparticles) may become a future interesting approach for in vivo CRISPR-Cas9 administration [59, 60].

Notwithstanding the utilisation of CRISPR-Cas9 plasmid vectors, no pertinent off-target occurrences were identified (Figs. S3, S4). However, deep sequencing analysis revealed the presence of substitutions distant to the expected Cas9 cleavage site, also in the non-transfected samples (Fig. S3). It is noteworthy that in all instances, the observed substitutions were transitions (A>G or T>C), which align with the anticipated error profile of the Phusion™ High-Fidelity DNA Polymerase utilized in library generation. Moreover, the frequency of these substitutions is below the polymerase's theoretical error threshold [61], (Table S3). Thus, it is critical to perform deeper and unbiased analysis such as whole genome sequencing prior the clinical application of this technology.

Our experiments demonstrate that the generated EditedΔ45–55 clone harbouring the del45–55-D1 is capable of restoring the DMD reading frame and dystrophin expression. The production of large deletions might disturb the genomic architecture and alter the splicing process impacting on the resultant proteins and the phenotype [62]. No alterations were observed in the edited clone's RNA, with the expected transcript comprising exon 44 and 56 sequences juxtaposed (Fig. 3A) being detected.

Dystrophin protein expression in the EditedΔ45–55 line was assessed by a range of techniques. Initially, immunofluorescence was employed to confirm the recovery of dystrophin and its correct location in the edited differentiated myotubes. The dystrophin quantification in all cell lines was evaluated using western blot analysis. Given the known variability in dystrophin expression even among healthy subjects [63], we incorporated

a total of 3 control cell lines. The restoration of dystrophin expression in the EditedΔ45–55 myotubes' was confirmed in comparison to the DMD unedited myotubes' (Fig. 4B). Due to the technical variability observed, a more precise and robust method for dystrophin quantification was employed: the in-cell western technique (myoblot) [44]. Once more, the restoration of dystrophin was confirmed in the edited myotubes, with levels comparable to those observed in the patient-derived ImΔ45–55-D1 myotubes (Fig. 4C). It is noteworthy that these cell lines exhibited elevated dystrophin levels (superior to those observed in C1 and C3), which aligns with previous studies examining dystrophin expression in patients with diverse in-frame DMD mutations [22, 64], including the del45–55 [27]. Additionally, the variable dystrophin expression across distinct healthy control cell lines was demonstrated.

Finally, a comprehensive examination of the myogenic capacity of the cell lines at various stages of the differentiation process was undertaken. The fusion index, myotube diameter, and the percentage of MyHC-positive cells were measured and found to indicate alterations in these parameters in the DMD cell line. Following gene editing (EditedΔ45–55), however, these parameters were restored to levels comparable to those observed in patient-derived myotubes. The analysis of the myogenic regulatory factors Myf5, MyoD, and Myh3 demonstrated the expected expression patterns (Fig. 6). However, the DMD cell line exhibited higher MyoD expression at d5 (Fig. 6B) and lower Myh3 levels than the other cell lines at the final stages of differentiation (Fig. 6C). These data suggest a defect in terminal myogenic differentiation in the DMD cell line, which was ameliorated with the introduction of the del45–55.

Conclusions

In conclusion, although many uncertainties still exist surrounding the clinical variability of the DMD del45–55, we have demonstrated as proof of concept, the potential

of mimicking specific intronic breaking points that are naturally present in a subgroup of subjects, the majority of whom exhibit a relatively benign phenotype. We have also recapitulated the ability of the versatile CRISPR-Cas9 system to create custom deletions, enabling the rescue of dystrophin expression as well as improving the altered phenotypes. Furthermore, the edited cell line was compared to the patient's immortalised myoblasts with the same deletion, allowing the characterisation and validation of both cellular models. Accordingly, we postulate that the cell lines generated in this study may serve as appropriate models for *in vitro* experimentation, with a view to resolving the remaining unsolved DMD pathogenic mechanisms.

Abbreviations

AON	Antisense oligonucleotide
BMD	Becker muscular dystrophy
ddPCR	Droplet digital PCR
DMD	Duchenne muscular dystrophy
FACS	Fluorescence activated cell sorter
MyHC	Myosin heavy chain
ORF	Open reading frame
RNP	Ribonucleoprotein
Myf5	Myogenic factor 5
MyoD	Myoblast determination protein 1

Supplementary Information

The online version contains supplementary material available at <https://doi.org/10.1186/s13395-024-00353-3>.

Supplementary Material 1

Acknowledgements

We strongly acknowledge the Fundación Isabel Gemio for supporting this work and for its enormous effort in securing funding, their trust in our work, and extraordinary cooperation. We acknowledge the use of cell cultures provided by the Institut de Myologie (Paris, France). We gratefully acknowledge the use of the antibodies provided by Professor Glenn Morris from the Muscular Dystrophy Association (MDA) Monoclonal Antibody Resource, which distributes antibodies for research in neuromuscular diseases worldwide from Oswestry, United Kingdom. The MF20 antibody developed by D.A. Fischman, Weill Cornell Medical College, was obtained from the Developmental Studies Hybridoma Bank, created by the NICHD of the NIH and maintained at the University of Iowa, Department of Biology, Iowa City, IA 52242. Cell sorting experiments were performed at the Cell Analytics Facility at Achucarro-Basque Centre of Neuroscience (Leioa, Spain).

Author contributions

Conceptualization, J.J.V., J.P.-G., R.P.V.-M., V.A.-G.; software, A.L., E.G.-R., G.G.-G.; methodology, validation, formal analysis and investigation, J.P.-G., P.S.-M., A.L., A. L.-M.; PM; E.G.-R., G.G.-G.; resources, A.L., R.P.V.-M., N.M., G.G.-G., J.O., V.A.-G.; writing—original draft preparation, J.P.-G., J.J.V.; writing—review and editing, J.P.-G., P.S.-M., A.L., A. L.-M.; E.G.-R., R.P.V.-M., N.M., G.G.-G., J.O., V.A.-G., J.J.V.; visualization, J.P.-G., P.S.-M., E.G.-R.; supervision, J.J.V., A.L., R.P.V.-M., V.A.-G.; project administration, J.J.V., V.A.-G. and funding acquisition, J.J.V., V.A.-G. All authors reviewed the manuscript and have agreed to the current manuscript version.

Funding

This work was possible thanks to the “Fundación Isabel Gemio” that funded the project and supported J. P.-G. with a PhD grant (2018/0200). Additional funding was received from Health Institute Carlos III (ISCIII, Spain): Grant PI15/00333; Basque Government (grants 2016111029, 2018222035 and 2020333012) and Duchenne Parent Project Spain (grant 05/2016). P. S.-M. acknowledges a Rio Hortega Fellowship from ISCIII (CM19/00104). A.L. has

two grants from the Generalitat Valenciana (GVA), APOSTD/2021/212 and CIGE/2021/015. A.L.-M. acknowledges funding by Biocruces Bizkaia Health Research Institute (BC/I/Div/19/001) and FPU Program of Spanish Ministry of Science, Research and Universities (FPU20/00912). R.P.V.-M. holds two grants from the ISCIII PI20/00114 and PI23/00455. N.M. acknowledges fundings from the ISCIII PI21/01532 and from the Generalitat Valenciana PROMETEO/2019/075. G. G.-G. acknowledges two grants from the ISCIII, CP22/00028 and PI22/01371, V.A.-G. acknowledges funding from a Miguel Servet Fellowship from the ISCIII (CPII17/00004), and from Ikerbasque (Basque Foundation for Science). All the funds from the ISCIII are partially supported by the European Regional Development Fund (ERDF/FEDER), ‘A way of making Europe’ from the EU.

Data availability

No datasets were generated or analysed during the current study.

Declarations

Ethics approval and consent to participate

All the experiments were approved by the Health Research Institute La Fe Ethics' Committee (ID: 2018/0200).

Consent for publication

Not applicable.

Competing interests

The authors declare no competing interests.

Author details

- ¹Neuromuscular and Ataxias Research Group, Health Research Institute Hospital La Fe (IIS La Fe), Valencia, Spain
- ²Centre for Biomedical Network Research on Rare Diseases (CIBERER), CB23/07/00005, Madrid, Spain
- ³University of Valencia, Valencia, Spain
- ⁴Nucleic Acid Therapeutics for Rare Disorders (NAT-RD), Biobizkaia Health Research Institute, Barakaldo, Spain
- ⁵Hematology Research Group, Health Research Institute Hospital La Fe (IIS La Fe), Valencia, Spain
- ⁶Centre for Biomedical Network Research on Cancer (CIBERONC), CB16/12/00284, Madrid, Spain
- ⁷Laboratory of Molecular, Cellular and Genomic Biomedicine, Health Research Institute Hospital La Fe, Valencia, Spain
- ⁸Centre for Biomedical Network Research on Rare Diseases (CIBERER), U755, CB06/07/1030, Madrid, Spain
- ⁹Joint Unit for Rare Diseases IIS La Fe-CIPF, Valencia, Spain
- ¹⁰Neuromuscular Referral Center, European Reference Network on Rare Neuromuscular Diseases (ERN EURO-NMD), Hospital Universitari I Politècnic La Fe, Valencia, Spain
- ¹¹Centre for Biomedical Network Research on Rare Diseases (CIBERER), U763, CB06/05/0091, Madrid, Spain
- ¹²Centre de Recherche en Myologie, Sorbonne Université, INSERM, Institut de Myologie, Paris 75013, France
- ¹³Ikerbasque, Basque Foundation for Science, Bilbao, Spain

Received: 7 January 2024 / Accepted: 13 September 2024

Published online: 01 October 2024

References

- Davies KE, Nowak KJ. Molecular mechanisms of muscular dystrophies: old and new players. *Nat Rev Mol Cell Biol*. 2006;7:762–73.
- Rando TA. The dystrophin-glycoprotein complex, cellular signaling, and the regulation of cell survival in the muscular dystrophies. *Muscle Nerve*. 2001;24:1575–94.
- Emery AEH. Population frequencies of inherited neuromuscular diseases—A world survey. *Neuromuscul Disord*. 1991;1:19–29.
- Emery AEH, Muntoni F, Quinlivan RCM. Duchenne muscular dystrophy. *OUP Oxford*; 2015.
- Darras BT, Urion DK, Ghosh PS. Dystrophinopathies. *GeneReviews*[®] [Internet]. 2022 [cited 2022 Jun 22];35. <https://www.ncbi.nlm.nih.gov/books/NBK1119/>

6. Bushby KMD, Thambyayah M, Gardner-Medwin D. Prevalence and incidence of Becker muscular dystrophy. *Lancet*. 1991;337:1022–4.
7. Ferreiro V, Giliberto F, Muñoz GMN, Francipane L, Marzese DM, Mampel A, et al. Asymptomatic Becker muscular dystrophy in a family with a multiexon deletion. *Muscle Nerve*. 2009;39:239–43.
8. Sanchez-Arjona MB. Spanish family with myalgia and cramps syndrome. *J Neurol Neurosurg Psychiatry*. 2005;76:286–9.
9. Nakamura A. X-Linked dilated cardiomyopathy: a cardiospecific phenotype of Dystrophinopathy. *Pharmaceuticals*. 2015;8:303–20.
10. North KN, Miller G, Iannaccone ST, Clemens PR, Chad DA, Bella I, et al. Cognitive dysfunction as the major presenting feature of Becker's muscular dystrophy. *Neurology*. 1996;46:461–4.
11. Nicolas A, Raguénès-Nicol C, Ben Yaou R, Ameziane-Le Hir S, Chéron A, Vié V, et al. Becker muscular dystrophy severity is linked to the structure of dystrophin. *Hum Mol Genet*. 2015;24:1267–79.
12. Bello L, Pegoraro E. The Usual suspects: genes for inflammation, fibrosis, regeneration, and muscle strength modify Duchenne muscular dystrophy. *J Clin Med*. 2019;8:649.
13. Verhaart IEC, Aartsma-Rus A. Therapeutic developments for Duchenne muscular dystrophy. *Nature Reviews Neurology*. 2019;15:373–86.
14. Tang A, Yokota T. Duchenne muscular dystrophy: promising early-stage clinical trials to watch. *Expert Opin Investig Drugs*. 2024;33:201–17.
15. Arechavala-Gomez V, Anthony K, Morgan J, Muntoni F. Antisense oligonucleotide-mediated exon skipping for Duchenne muscular dystrophy: Progress and challenges. *Curr Opin Ther Ther*. 2012;12:152–60.
16. Nelson CE, Hakim CH, Ousterout DG, Thakore PI, Moreb EA, Rivera RMC et al. In vivo genome editing improves muscle function in a mouse model of Duchenne muscular dystrophy. *Science* (1979). 2016;351:403–7.
17. Long C, Amoasii L, Mireault AA, McAnally JR, Li H, Sanchez-Ortiz E et al. Postnatal genome editing partially restores dystrophin expression in a mouse model of muscular dystrophy. *Science* (1979). 2016;351:400–3.
18. Amoasii L, Hildyard JCW, Li H, Sanchez-Ortiz E, Mireault A, Caballero D et al. Gene editing restores dystrophin expression in a canine model of Duchenne muscular dystrophy. *Science* (1979). 2018;362:86–91.
19. Tabebordbar M, Cheng J, Wagers AJ. Therapeutic Gene Editing in Muscles and Muscle Stem Cells. *Research and Perspectives in Neurosciences*. 2017;103–23.
20. Duan D. Systemic AAV micro-dystrophin gene therapy for Duchenne muscular dystrophy. *Mol Ther*. 2018;26:2337–56.
21. Hammond SM, Aartsma-Rus A, Alves S, Borgos SE, Buijsen RAM, Collin RWJ et al. Delivery of oligonucleotide-based therapeutics: challenges and opportunities. *EMBO Mol Med*. 2021;13:e13243.
22. Anthony K, Cirak S, Torelli S, Tascia G, Feng L, Arechavala-Gomez V, et al. Dystrophin quantification and clinical correlations in Becker muscular dystrophy: implications for clinical trials. *Brain*. 2011;134:3544–56.
23. Anthony K, Arechavala-Gomez V, Ricotti V, Torelli S, Feng L, Janghra N et al. Biochemical Characterization of Patients With In-Frame or Out-of-Frame DMD Deletions Pertinent to Exon 44 or 45 Skipping. *JAMA Neurol*. 2014;71:32.
24. Nakamura A, Shiba N, Miyazaki D, Nishizawa H, Inaba Y, Fueki N, et al. Comparison of the phenotypes of patients harboring in-frame deletions starting at exon 45 in the Duchenne muscular dystrophy gene indicates potential for the development of exon skipping therapy. *J Hum Genet*. 2017;62:459–63.
25. Flanigan KM, Dunn DM, von Niederhausern A, Soltanzadeh P, Gappmaier E, Howard MT, et al. Mutational spectrum of DMD mutations in dystrophinopathy patients: application of modern diagnostic techniques to a large cohort. *Hum Mutat*. 2009;30:1657–66.
26. Bérout C, Tuffery-Giraud S, Matsuo M, Hamroun D, Humbertclaude V, Monnier N, et al. Multiexon skipping leading to an artificial DMD protein lacking amino acids from exons 45 through 55 could rescue up to 63% of patients with Duchenne muscular dystrophy. *Hum Mutat*. 2007;28:196–202.
27. Poyatos-García J, Martí P, Liquori A, Muelas N, Pitarch I, Martínez-Dolz L et al. Dystrophinopathy Phenotypes and Modifying Factors in DMD Exon 45–55 Deletion. *Ann Neurol*. 2022;92:793–806.
28. Aoki Y, Yokota T, Nagata T, Nakamura A, Tanihata J, Saito T et al. Bodywide skipping of exons 45–55 in dystrophic mdx52 mice by systemic antisense delivery. *Proceedings of the National Academy of Sciences*. 2012;109:13763–8.
29. Echigoya Y, Aoki Y, Miskew B, Panesar D, Touznik A, Nagata T, et al. Long-term efficacy of systemic multiexon skipping targeting dystrophin exons 45–55 with a cocktail of vivo-morpholinos in Mdx52 mice. *Mol Ther Nucleic Acids*. 2015;4:e225.
30. Lee J, Echigoya Y, Duddy W, Saito T, Aoki Y, Takeda ichi et al. Antisense PMO cocktails effectively skip dystrophin exons 45–55 in myotubes transdifferentiated from DMD patient fibroblasts. 2018;13(5):e0197084.
31. Echigoya Y, Lim KRQ, Melo D, Bao B, Trieu N, Mizobe Y, et al. Exons 45–55 skipping using mutation-tailored cocktails of antisense morpholinos in the DMD Gene. *Mol Ther*. 2019;27:2005–17.
32. Ousterout DG, Kabadi AM, Thakore PI, Majoros WH, Reddy TE, Gersbach CA. Multiplex CRISPR/Cas9-based genome editing for correction of dystrophin mutations that cause Duchenne muscular dystrophy. *Nat Commun*. 2015;6:6244.
33. Young CS, Hicks MR, Ermolova NV, Nakano H, Jan M, Younesi S, et al. A single CRISPR-Cas9 deletion strategy that targets the majority of DMD patients restores dystrophin function in hiPSC-Derived muscle cells. *Cell Stem Cell*. 2016;18:533–40.
34. Young CS, Mokhonova E, Quinonez M, Pyle AD, Spencer MJ. Creation of a Novel Humanized Dystrophic Mouse Model of Duchenne muscular dystrophy and application of a CRISPR/Cas9 gene editing therapy. *J Neuromuscul Dis*. 2017;4:139–45.
35. Thorley M, Duguez S, Mazza EMC, Valsoni S, Bigot A, Mamchaoui K, et al. Skeletal muscle characteristics are preserved in hTERT/cdk4 human myogenic cell lines. *Skelet Muscle*. 2016;6:1–12.
36. Mamchaoui K, Trollet C, Bigot A, Negroni E, Chaouch S, Wolff A, et al. Immortalized pathological human myoblasts: towards a universal tool for the study of neuromuscular disorders. *Skelet Muscle*. 2011;1:34.
37. Soblecherro-Martín P, Albiásu-Arteta E, Anton-Martínez A, de la Puente-Ovejero L, García-Jiménez I, González-Iglesias G et al. Duchenne muscular dystrophy cell culture models created by CRISPR/Cas9 gene editing and their application in drug screening. *Sci Rep*. 2021;11:18188.
38. Sabater-Arcis M, Bargiela A, Moreno N, Poyatos-García J, Vilchez JJ, Artero R. Musashi-2 contributes to myotonic dystrophy muscle dysfunction by promoting excessive autophagy through miR-7 biogenesis repression. *Mol Ther Nucleic Acids*. 2021;25:652–67.
39. Poyatos-García J, Blázquez-Bernal Á, Selva-Giménez M, Bargiela A, Espinosa-Espinosa J, Vázquez-Manrique RP et al. CRISPR-Cas9 editing of a TNPO3 mutation in a muscle cell model of limb-girdle muscular dystrophy type D2. *Mol Ther Nucleic Acids*. 2023;31:324–38.
40. Ran FA, Hsu PD, Wright J, Agarwala V, Scott DA, Zhang F. Genome engineering using the CRISPR-Cas9 system. *Nat Protocols*. 2013;8:11.
41. Fuster-García C, García-García G, González-Romero E, Jaijo T, Sequedo MD, Ayuso C, et al. USH2A gene editing using the CRISPR System. *Mol Ther Nucleic Acids*. 2017;8:529–41.
42. Bae S, Park J, Kim J-S. Cas-OFFinder: a fast and versatile algorithm that searches for potential off-target sites of Cas9 RNA-guided endonucleases. *Bioinformatics*. 2014;30:1473–5.
43. López-Martínez A, Soblecherro-Martín P, Arechavala-Gomez V. Evaluation of Exon Skipping and Dystrophin Restoration in In Vitro Models of Duchenne Muscular Dystrophy. Arechavala-Gomez V, Garanto A, editors. *Methods Mol Biol*. 2022;2434:217–33.
44. Ruiz-Del-Yerro E, García-Jiménez I, Mamchaoui K, Arechavala-Gomez V. Myoblots: dystrophin quantification by in-cell western assay for a streamlined development of Duchenne muscular dystrophy (DMD) treatments. *Neuro-pathol Appl Neurobiol*. 2018;44:463–73.
45. Anthony K, Arechavala-Gomez V, Taylor LE, Vulin A, Kaminoh Y, Torelli S, et al. Dystrophin quantification: Biological and translational research implications. *Neurology*. 2014;83:2062–9.
46. Oliveros JC, Franch M, Tabas-Madrid D, San-León D, Montoliu L, Cubas P, et al. Breaking-Cas—interactive design of guide RNAs for CRISPR-Cas experiments for ENSEMBL genomes. *Nucleic Acids Res*. 2016;44:W267–71.
47. Clement K, Rees H, Canver MC, Gehrke JM, Farouni R, Hsu JY, et al. CRISPResso2 provides accurate and rapid genome editing sequence analysis. *Nat Biotechnol*. 2019;37:224–6.
48. Chal J, Pourquie O. Making muscle: skeletal myogenesis in vivo and in vitro. *Development*. 2017;144:2104–22.
49. Schmidt M, Schüller SC, Hüttner SS, von Eyss B, von Maltzahn J. Adult stem cells at work: regenerating skeletal muscle. *Cellular and Molecular Life Sciences*. 2019;76:2559–70.
50. Zhang H, Shang R, Bi P. Feedback regulation of Notch signaling and myogenesis connected by MyoD-Dll1 axis. *PLoS Genet*. 2021;17:e1009729.
51. Doorenweerd N, Straathof CS, Dumas EM, Spitali P, Ginjaar IB, Wokke BH, et al. Reduced cerebral gray matter and altered white matter in boys with Duchenne muscular dystrophy. *Ann Neurol*. 2014;76:403–11.

52. Felisari G, Boneschi FM, Bardoni A, Sironi M, Comi GP, Robotti M, et al. Loss of Dp140 dystrophin isoform and intellectual impairment in Duchenne dystrophy. *Neurology*. 2000;55:559–64.
53. Gargaun E, Falcone S, Solé G, Durigneux J, Urtizberea A, Cuisset JM, et al. The lncRNA 44s2 study applicability to the design of 45–55 exon skipping therapeutic strategy for DMD. *Biomedicines*. 2021;9:219.
54. Lidov HGW, Selig S, Kunkel LM. Dp140: a novel 140 kDa CNS transcript from the dystrophin locus. *Hum Mol Genet*. 1995;4:329–35.
55. Bovolenta M, Erriquez D, Valli E, Brioschi S, Scotton C, Neri M, et al. The DMD Locus Harbours multiple long non-coding RNAs which orchestrate and Control Transcription of Muscle Dystrophin mRNA isoforms. *PLoS ONE*. 2012;7:e45328.
56. Wojtal D, Kemaladewi DU, Malam Z, Abdullah S, Wong TWY, Hyatt E, et al. Spell checking Nature: versatility of CRISPR/Cas9 for developing treatments for inherited disorders. *Am J Hum Genet*. 2016;98:90–101.
57. Zhang S, Shen J, Li D, Cheng Y. Strategies in the delivery of Cas9 ribonucleoprotein for CRISPR/Cas9 genome editing. *Theranostics*. 2021;11:614–48.
58. Kim S, Kim D, Cho SW, Kim J, Kim JS. Highly efficient RNA-guided genome editing in human cells via delivery of purified Cas9 ribonucleoproteins. *Genome Res*. 2014;24:1012–9.
59. Li L, Hu S, Chen X. Non-viral delivery systems for CRISPR/Cas9-based genome editing: challenges and opportunities. *Biomaterials*. 2018;171:207–18.
60. Taha EA, Lee J, Hotta A. Delivery of CRISPR-Cas tools for in vivo genome editing therapy: Trends and challenges. *J Controlled Release*. 2022;342:345–61.
61. Mcinerney P, Adams P, Hadi MZ. Error Rate Comparison during Polymerase Chain Reaction by DNA Polymerase. 2014;204:287430.
62. Tuffery-Giraud S, Miro J, Koenig M, Claustres M. Normal and altered pre-mRNA processing in the DMD gene. *Hum Genet*. 2017;136:1155–72.
63. Arechavala-Gomez V, Kinali M, Feng L, Brown SC, Sewry C, Morgan JE, et al. Immunohistological intensity measurements as a tool to assess sarcolemma-associated protein expression. *Neuropathol Appl Neurobiol*. 2009;36:265–74.
64. van den Bergen JC, Wokke BH, Janson AA, van Duinen SG, Hulsker MA, Ginjaar HB et al. Dystrophin levels and clinical severity in Becker muscular dystrophy patients. *J Neurol Neurosurg Psychiatry*. 2014;85:747–53.

Publisher's note

Springer Nature remains neutral with regard to jurisdictional claims in published maps and institutional affiliations.